Tale of J1328+2752: a misaligned double–double radio galaxy hosted by a binary black hole?

S. Nandi,[1][*] M. Jamrozy,[2][*] R. Roy,[3][*] J. Larsson,[1] D. J. Saikia,[4,5] M. Baes[6] and M. Singh[7]

[1]*Department of Physics, KTH, The Oskar Klein Centre, AlbaNova, SE-106 91 Stockholm, Sweden*
[2]*Obserwatorium Astronomiczne, Uniwersytet Jagielloński, ul. Orla 171, PL-30-244 Kraków, Poland*
[3]*Department of Astronomy, Stockholm University, The Oskar Klein Centre, AlbaNova, SE-10691 Stockholm, Sweden*
[4]*Cotton College State University, Panbazar, Guwahati 781 001, India*
[5]*National Centre for Radio Astrophysics, TIFR, Pune University Campus, Post Bag 3, Pune 411 007, India*
[6]*Sterrenkundig Observatorium, Universiteit Gent, Krijgslaan 281 S9, B-9000 Gent, Belgium*
[7]*Aryabhatta Research Institute of Observational Sciences (ARIES), Manora Peak, Nainital, 263 129, India*

ABSTRACT

We present a radio and optical study of the double–double radio galaxy J1328+2752 based on new low-frequency Giant Metrewave Radio Telescope observations and Sloan Digital Sky Survey (SDSS) data. The radio data were used to investigate the morphology and to perform a spectral index analysis. In this source, we find that the inner double is misaligned by $\sim 30°$ from the axis of the outer diffuse structure. The SDSS spectrum shows that the central component has double-peaked line profiles with different emission strengths. The average velocity offset of the two components is $235 \pm 10.5\,\mathrm{km\,s^{-1}}$. The misaligned radio morphology along with the double-peaked emission lines indicate that this source is a potential candidate binary supermassive black hole. This study further supports mergers as a possible explanation for repeated jet activity in radio sources.

Key words: line: identification – line: profiles – galaxies: active – galaxies: individual: J1328+2752 – galaxies: nuclei – radio continuum: galaxies.

1 INTRODUCTION

The existence of two or more pairs of synchrotron emitting radio lobes driven by the same central active galactic nucleus (AGN) is extremely important for understanding the evolution of AGNs, as it provides vital evidence for multiple episodes of nuclear activity. Such sources are often termed double-double radio galaxies (DDRGs) (Schoenmakers et al. 2000). These DDRGs exhibit a wide range of linear sizes, from less than few hundreds of kpc up to more than a Mpc (Saikia & Jamrozy 2009; Nandi & Saikia 2012; Konar & Hardcastle 2013). For these episodic sources, the new jets usually follow the same direction as the previous jets. There are a few examples of 'misaligned DDRGs' that have different orientation of axes for the two epochs. Saikia, Konar & Kulkarni (2006) show that the misalignment angle is within $\sim 20°$ for a sample of 12 DDRGs. However, the steep-spectrum core-dominated radio galaxy 3C293 provides excellent observational evidence of restarted jet activity along with an $\sim 35°$ jet rotation (Akujor et al. 1996). The estimated time-scale of episodic activity in 3C293 is $\sim 10^5$ yr, which is significantly smaller than most

other known DDRGs (Joshi et al. 2011). In accordance with this, Machalski et al. (2016) found that the outer lobes are ~ 60 Myr old and that the jet activity related to the formation of the outer lobes ceased within the last Myr. Meanwhile, the misaligned inner lobes are only about ~ 0.3 Myr old. The derived jet time-scales provide strong support for the Lense–Thirring precession model (Bardeen & Petterson 1975), in which the supermassive black hole (SMBH) spin, and therefore the jet axis, flips rapidly. Recently, Saripalli et al. (2013) identified another DDRG, B0707-359, with a misalignment angle of about $\sim 30°$ between the two epochs of activity.

The reorientation of the jet axis in these misaligned DDRGs may be caused by an axis precession or axis flip of the AGN. Influence of a nearby galaxy or the coalescence of massive black holes may trigger a new jet with sufficient axis rotation to explain the observations (Roberts, Saripalli & Subrahmanyan 2015). Historically, radio galaxies with a rapid change of jet direction, in particular, 'X-shaped' galaxies, have been proposed as candidates for binary black holes (see e.g. Begelman, Blandford & Rees 1980; Murgia et al. 2001; Lal & Rao 2007; Roberts et al. 2015). These sources are also promising contributors to the gravitational wave background (Begelman et al. 1980; Abbott et al. 2016). Recently, double-peaked emission lines in AGN have been suggested as an indicator for binary black holes. Such lines are a possible signature of a bound pair of SMBHs, moving with their own characteristic velocities (Fu

[*] E-mail: sumana1981@gmail.com (SN); jamrozy@oa.uj.edu.pl (MJ); rupak.roy@astro.su.se (RR)
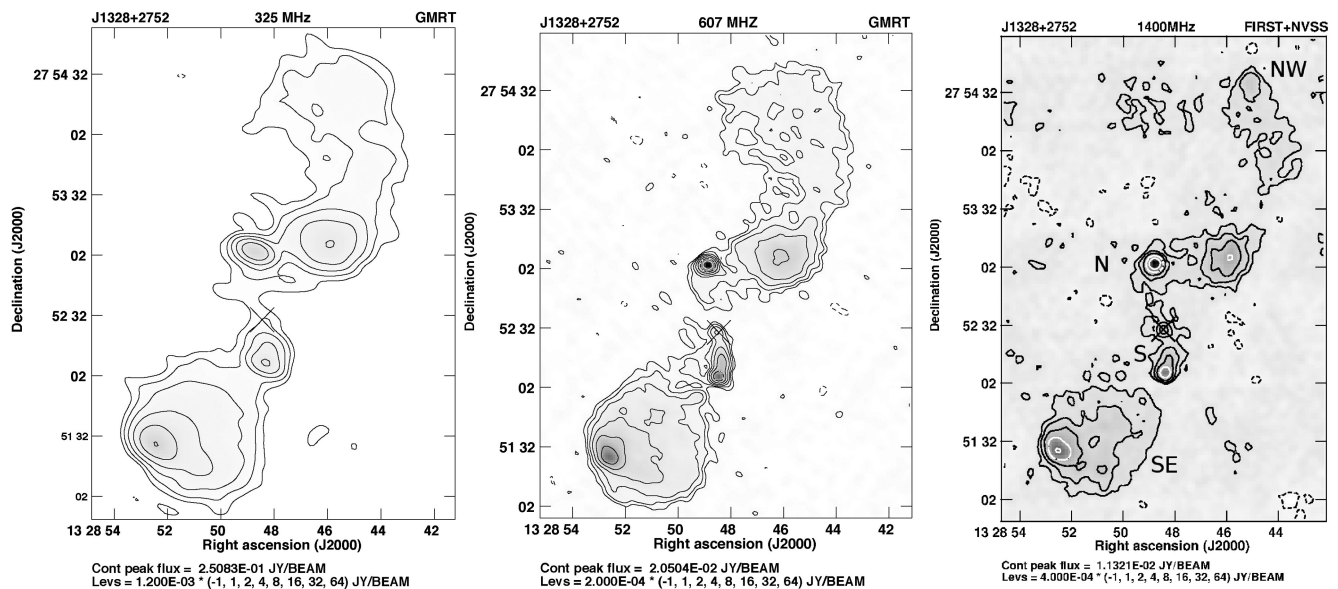
Figure 1. Images of J1328+2752 at 325, 607 and 1400 MHz. The position of the optical host is marked with a '×'. The locations of the different components are marked in the 1400 MHz map. The image details are presented in Table 2.

et al. 2011; Woo et al. 2014; Kharb et al. 2015). However, apart from binary black holes, there are other scenarios that may explain double-peaked emission lines, including jet–cloud interactions or rotating gaseous disk (Smith et al. 2012). Of these different possibilities, the scenario of binary black holes is more likely in the case of merger remnants or elliptical galaxies (Deane et al. 2014). A misaligned DDRG hosted by a giant elliptical with double-peaked emission lines is therefore of great interest as a potential candidate for harbouring a binary black hole. Such systems may provide direct observational evidence for galaxy mergers as triggers of multiple epochs of jet activity (Nandi et al. 2014).

From our previous study (Nandi & Saikia 2012), we have identified one such source, J1328+2752. This system shows not only restarted jet activity with an axis reorientation, but also double-peaked emissions lines from the central AGN at a redshift 0.0911. Ge et al. (2012) included the host galaxy of J1328+2752 in a list of 3030 galaxies that show double-peaked narrow emission-lines in their 'Sloan Digital Sky Survey' (SDSS) spectra. The linear sizes of the inner and outer doubles of this source are 96 and 413 kpc, respectively. In this Letter, we present new low-frequency radio observations of J1328+2752 along with a study of the optical spectrum. We assume a Universe with $H_0 = 71 \, \text{km} \, \text{s}^{-1} \, \text{Mpc}^{-1}$, $\Omega_m = 0.27$ and $\Omega_{vac} = 0.73$.

2 OBSERVATIONS AND DATA ANALYSIS

Both radio and optical data have been used to analyse the characteristics of J1328+2752.

Radio data: the radio observations were performed with the Giant Metrewave Radio Telescope (GMRT) under proposal codes 23_056 and 28_044. The target was observed on 2013-03-24 for 3.6 h at 607 MHz and on 2015-06-27 for 4.7 h at 325 MHz. We observed the flux density calibrator, 3C286, at the beginning and end of each observing run and also used it as a bandpass calibrator based on the scale of Baars et al. (1977). The phase calibrator, J1330+251, was observed for ∼5 min after each of several ∼20 min exposures of J1328+2752. We used the AIPS software package for data reduction.

Table 1. Integrated flux densities.

Obs. freq. (MHz) (1)	S (mJy) (2)	Error (mJy) (3)	Survey used (4)	Ref used (5)
74	1457	208	VLSSr	(1)
151	800	117	7C	(2)
325	627	94	GMRT	(3)
408	529	72	B2	(4)
607	414	29	GMRT	(3)
1400	247	25	GB	(5)
1400	249	13	NVSS	(6)
1400	152	8	FIRST	(7)
1400	206	10		(8)
4850	85	12	87GB	(9)

Notes. Column 1 gives the frequency, Columns 2 and 3 give the total flux densities of the source and the flux density error, Column 4 gives the name of the survey, Column 5 gives references – (1) Lane et al. (2014) (the original flux density of the VLSSr survey was multiplied by a factor of 0.9 to be consistent with the Baars et al. 1977 scale), (2) Waldram et al. (1996), (3) our observation, (4) Colla et al. (1972), (5) White & Becker (1992), (6) Condon et al. (1998), (7) White et al. (1997), (8) combined NVSS and FIRST from this Letter, (9) Gregory & Condon (1991).

To obtain the best possible images, several rounds of self-calibration were performed.

For this study, we also used images at 1400 MHz obtained from FIRST (Faint Images of the Radio Sky at Twenty centimetres; Becker, White & Helfand 1995) and NVSS (NRAO VLA Sky Survey; Condon et al. 1998). Since about 40 per cent of the flux density (and structure) is lost in the high-resolution FIRST map, the FIRST and NVSS images were combined to image the range of structure shown in Fig. 1. The final merged map was checked for flux density consistency by comparing the flux density of point sources in the FIRST and merged maps. This difference did not exceed 1 per cent. The integrated flux densities at different frequencies are given in Table 1. Additionally, we used the NVSS Q and U Stokes maps

Table 2. Observational parameters and flux densities.

Freq. (MHz) (1)	Beam size (arcsec) (2)	(arcsec) (3)	(°) (4)	rms (mJy b⁻¹) (5)	Cmp. (6)	S_p (mJy b⁻¹) (7)	S_t (mJy) (8)
G325	13.15	7.18	69	0.38	NW	19.5	239
					N	37	44
					C		$\lesssim$1.5
					S	21	48
					SE	39	296
G607	5.27	4.22	69	0.07	NW	3.5	164
					N	20	28
					C	1.8	2
					S	11	29
					SE	11	193
V1400	5.40	5.40	0	0.19	NW	3.3	73
					N	11	19
					C	2	2
					S	5	18
					SE	7	95

Notes. Column 1: frequency of observations where G and V indicate GMRT and VLA respectively; Columns 2–4: beam size in arcseconds and its PA in degrees; Column 5: rms in units of mJy beam⁻¹; Column 6: component designation, where NW, N, S and SE denote north-west outer, north inner, south inner and south-east outer components, respectively. C represents the central component. Columns 7, 8: the peak flux densities and total flux densities measured from the total intensity maps for each component in units of mJy beam⁻¹ and mJy, respectively.

and the AIPS task COMB to create images of the linearly polarized intensity and fractional polarization.

Optical data: the optical spectrum of J1328+2752 was obtained from data release DR12 of the SDSS (Alam et al. 2015). The observed spectrum is contaminated by the stellar absorption features of the host galaxy and also affected by the foreground extinction and recession velocity of the system. Before analysing the narrow emission lines, we have therefore removed all other features using the penalized pixel-fitting tool (pPXF; Cappellari & Emsellem 2004).

3 RESULTS

The full-resolution maps at 325, 607 and 1400 MHz are shown in Fig. 1. All these images show a new, inner structure centred at the optical host but about ∼30° off the axis of the earlier diffuse emission. The central radio core is visible at 1400 MHz. For the GMRT images, weak emission from the core is detected at 607 MHz, while the 325 MHz map does not show any clear core emission. The flux density values (see Table 2) of the central component indicate that this is a flat-spectrum radio core. The outer lobes are asymmetric in morphology. A bright hotspot in the southern outer lobe is visible at all three frequencies, while there is no evidence of a hotspot in the northern outer lobe. In the GMRT images, we note a sharp bend of the northern outer lobe towards the north-east and an enhancement of flux density at the position where the lobe starts to bend. The combined 1400 MHz image also shows an enhancement of flux density at the same position. The asymmetric inner double is completely embedded in the older diffuse emission. The northern inner component is dominated by a bright hotspot, while the southern inner component has an elongated structure with a bright hotspot at the end. The integrated flux densities and those of the components are presented in Tables 1 and 2, respectively, and plotted in Fig. 2, upper panel. The estimated spectral index α ($S_\nu \propto \nu^{-\alpha}$) for the whole source using only the low-resolution values at 1400 MHz is 0.63 ± 0.03. Ensuring that no flux density is
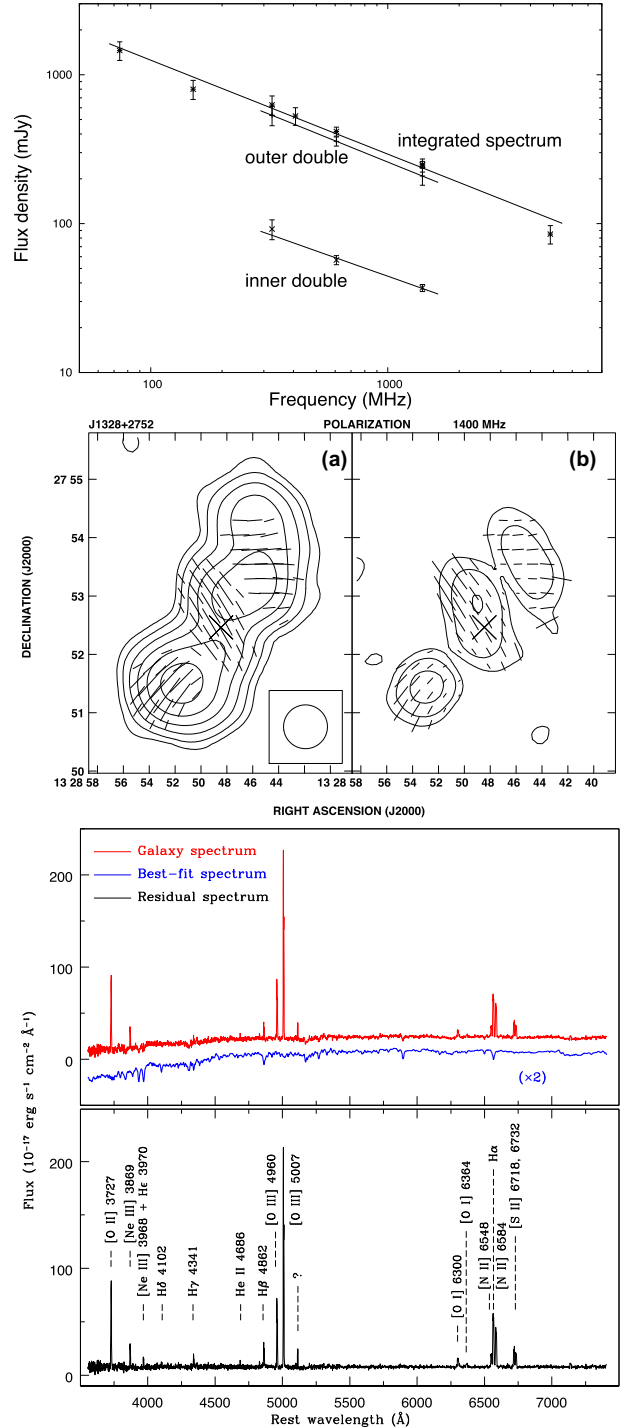

Figure 2. Upper panel: radio spectra of the whole source and the individual components. Middle panel: 1400 MHz NVSS polarimetric images. (a) Total intensity contours spaced by a factor of 2 starting at 1.35 mJy beam⁻¹. Superimposed are E-vectors with their lengths proportional to the polarized intensity, where 10 arcsec correspond to 1 mJy beam⁻¹. (b) Linearly polarized intensity contours spaced by a factor of 2 starting with 0.9 mJy beam⁻¹, with the vectors of the fractional linear polarization superimposed. A length of 10 arcsec corresponds to 10 per cent of the fractional linear polarization. The '×' marks the position of the host galaxy. Lower panel: redshift-corrected SDSS spectrum of the galaxy (in red) and the best-fitting model spectrum for the underlying stellar population of the host produced by pPXF (in blue)(upper half). Lower panel: the residual spectrum with the strongest emission lines labelled (lower half).
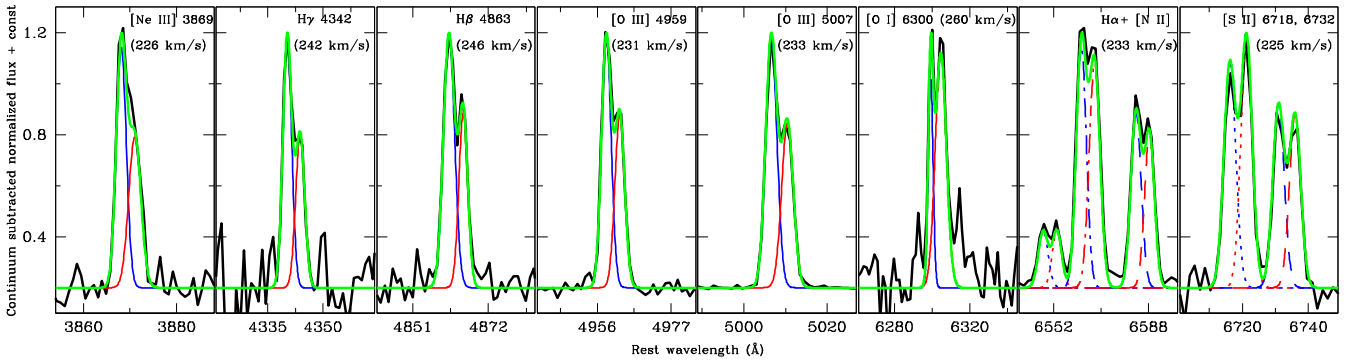
Figure 3. The double-peaked emission lines obtained from the de-reddened SDSS spectrum of J1328+2752. The velocity separations determined for each pair of lines are included in the upper, right corners of the panels.

missing, the spectral indices of the outer and inner doubles between 325 and 1400 MHz are 0.64 ± 0.002 and 0.56 ± 0.06, respectively.

The total intensity NVSS map with the electric field E-vectors superimposed is shown in Fig. 2, middle panel (a). The Fig. 2, middle panel (b) shows the linearly polarized intensity map with the vectors of fractional linear polarization superimposed. It can be seen that the whole structure is polarized. There are three distinct regions visible in the polarimetric maps. The total integrated polarized flux density of this source is 17.6 ± 1.4 mJy, which gives ∼7 per cent for the mean fractional polarization.

The optical spectrum (Fig. 2, lower panel) shows that J1328+2752 has an elliptical host with high-ionization narrow emission lines. The typical stellar velocity dispersion of the host determined using pPXF is 193.1 ± 13.6 km s^{-1}. This is consistent with the result from the SDSS DR12 survey (velocity dispersion 176.8 ± 9.7 km s^{-1}). A close inspection shows that the strong emission lines of J1328+2752 are double-peaked. Each continuum-subtracted emission line was deblended with two Gaussian functions using the IRAF routine SPLOT.[1] The continuum-subtracted normalized flux of 11 major emission lines are shown together with the normalized model in Fig. 3. The lines are [Ne III] λ3869, Hγ λ4342, Hβ λ4863, [O III] λ4959, [O III] λ5007, [O I] λ6300, Hα λ6563, [N II] λλ6548, 6584, and [S II] λλ6718, 6732. The left (blue) and right (red) Gaussian may correspond to two merging components. The total model flux (green) of each spectral line is also shown in the Fig. 3. After fitting these lines, we find that the two components are separated by a velocity of 235 ± 10.5 km s^{-1}. Such a velocity separation between the blue and red components is consistent with a scenario of two cores in merging galaxies (Woo et al. 2014). For every line, the intensities of the two narrow-line components are different. To understand the classes of the two merging components, we use the BPT diagnostic diagram (Baldwin, Phillips & Terlevich 1981; Kewley et al. 2006) shown in Fig. 4. This analysis distinguishes AGN characteristics from those of star-forming and composite galaxies using line ratios. The [N II]/Hα and [O III]/Hβ ratios calculated for the two components place them at nearby locations in the BPT diagram. This makes the possibility of 'jet–cloud interaction' quite unlikely and almost rules out the 'rotating-disk' scenario (Smith et al. 2012). It also indicates that this is a system of two merging AGNs.

The stellar velocity dispersion can be used to estimate the black hole mass through the relation given by Tremaine et al. (2002).
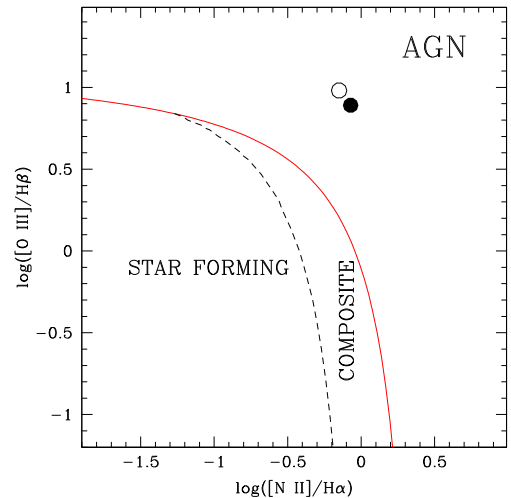
Figure 4. BPT diagram of J1328+2752. Open and filled circles represent the blue and red components of the system. The solid line separates star-forming galaxies and AGNs. Composite galaxies occupy the region between the dashed and solid lines.

For J1328+2752, the SDSS velocity dispersion gives a mass for the central black hole (or black hole pair) of $\log(M_{BH}/M_{\odot}) = 7.91 \pm 0.17$. This value is not as large as most SMBH masses in powerful radio galaxies, although objects of similar masses do exist (Kozieł-Wierzbowska & Stasińska 2011).

4 DISCUSSIONS AND CONCLUSIONS

We have presented 325 and 607 MHz GMRT continuum observations of J1328+2752. These data, together with the 1400 MHz image, reveal that the source has four distinct components in addition to a flat-spectrum core. The spectral indices of the outer double is steeper than the inner one, which indicate two epochs of jet activity (e.g. Konar et al. 2012; Konar & Hardcastle 2013; Orrù et al. 2015), although the difference here is small due to an active hotspot in the southern outer lobe and possible re-acceleration in the sharp bend in the northern outer lobe. From the radio morphology and spectral index analysis, we confirm this source as a DDRG with an axis rotation. The percentage of polarized emission is similar to that observed for X-shaped radio galaxies that show jet reorientation (e.g. Kozieł-Wierzbowska et al. 2012). Here we speculate that the different strengths of the two components of the optical emission lines is an indication that the system is associated with

two distinct narrow-line regions orbiting around each of two separate nuclei, plausibly constituted by a merging massive black hole binary. This source may therefore be a relevant candidate for future gravitational wave experiments. Moreover, this study supports the scenario that renewed jet activity may be associated with merger events. However, this dual black hole system cannot be spatially resolved by current available data. We plan for very long baseline interferometry (VLBI) imaging and high-angular resolution optical imaging to reveal the existence of a massive dual/binary black hole. It is possible to identify radio-emitting binary black holes with parsec-scale separations through VLBI (Deane et al. 2014). A linear separation by more than 8 or 3 pc of presumably two radio cores of J1328+2752 can be revealed, respectively, through 1600 or 5000 MHz VLBI observations.

ACKNOWLEDGEMENTS

REFERENCES

Abbott B. P. et al., 2016, Phys. Rev. Lett., 116, 241103
Akujor C. E., Leahy J. P., Garrington S. T., Sanghera H., Spencer R. E., Schilizzi R. T., 1996, MNRAS, 278, 1
Alam S. et al., 2015, ApJS, 219, 12
Baars J. W. M., Genzel R., Pauliny-Toth I. I. K., Witzel A., 1977, A&A, 61, 99
Baldwin J. A., Phillips M. M., Terlevich R., 1981, PASP, 93, 5
Bardeen J. M., Petterson J. A., 1975, ApJ, 195, L65
Becker R. H., White R. L., Helfand D. J., 1995, ApJ, 450, 559
Begelman M. C., Blandford R. D., Rees M. J., 1980, Nature, 287, 307
Cappellari M., Emsellem E., 2004, PASP, 116, 138
Colla G. et al., 1972, A&AS, 7, 1
Condon J. J., Cotton W. D., Greisen E. W., Yin Q. F., Perley R. A., Taylor G. B., Broderick J. J., 1998, AJ, 115, 1693
Deane R. P. et al., 2014, Nature, 511, 57
Fu H., Myers A. D., Djorgovski S. G., Yan L., 2011, ApJ, 733, 103
Ge J.-Q., Hu C., Wang J.-M., Bai J.-M., Zhang S., 2012, ApJS, 201, 31
Gregory P. C., Condon J. J., 1991, ApJS, 75, 1011
Joshi S. A., Nandi S., Saikia D. J., Ishwara-Chandra C. H., Konar C., 2011, MNRAS, 414, 1397
Kewley L. J., Groves B., Kauffmann G., Heckman T., 2006, MNRAS, 372, 961
Kharb P., Das M., Paragi Z., Subramanian S., Chitta L. P., 2015, ApJ, 799, 161
Konar C., Hardcastle M. J., 2013, MNRAS, 436, 1595
Konar C., Hardcastle M. J., Jamrozy M., Croston J. H., Nandi S., 2012, MNRAS, 424, 1061
Kozieł-Wierzbowska D., Stasińska G., 2011, MNRAS, 415, 1013
Kozieł-Wierzbowska D., Jamrozy M., Zola S., Stachowski G., Kuźmicz A., 2012, MNRAS, 422, 1546
Lal D. V., Rao A. P., 2007, MNRAS, 374, 1085
Lane W. M., Cotton W. D., van Velzen S., Clarke T. E., Kassim N. E., Helmboldt J. F., Lazio T. J. W., Cohen A. S., 2014, MNRAS, 440, 327
Machalski J., Jamrozy M., Stawarz Ł., Weżgowiec M., 2016, A&A, 595, A46
Murgia M., Parma P., de Ruiter H. R., Bondi M., Ekers R. D., Fanti R., Fomalont E. B., 2001, A&A, 380, 102
Nandi S., Saikia D. J., 2012, Bull. Astron. Soc. India, 40, 121
Nandi S. et al., 2014, ApJ, 789, 16
Orrù E. et al., 2015, A&A, 584, A112
Roberts D. H., Saripalli L., Subrahmanyan R., 2015, ApJ, 810, L6
Saikia D. J., Jamrozy M., 2009, B. Astron. Soc. India, 37, 63
Saikia D. J., Konar C., Kulkarni V. K., 2006, MNRAS, 366, 1391
Saripalli L., Malarecki J. M., Subrahmanyan R., Jones D. H., Staveley-Smith L., 2013, MNRAS, 436, 690
Schoenmakers A. P., de Bruyn A. G., Röttgering H. J. A., van der Laan H., Kaiser C. R., 2000, MNRAS, 315, 371
Smith K. L., Shields G. A., Salviander S., Stevens A. C., Rosario D. J., 2012, ApJ, 752, 63
Tremaine S. et al., 2002, ApJ, 574, 740
Waldram E. M., Yates J. A., Riley J. M., Warner P. J., 1996, MNRAS, 282, 779
White R. L., Becker R. H., 1992, ApJS, 79, 331
White R. L., Becker R. H., Helfand D. J., Gregg M. D., 1997, ApJ, 475, 479
Woo J.-H., Cho H., Husemann B., Komossa S., Park D., Bennert V. N., 2014, MNRAS, 437, 32

This paper has been typeset from a TEX/LATEX file prepared by the author.